Temperature measurements of shocked silica aerogel foam

K. Falk,[1] C. A. McCoy,[2] C. L. Fryer,[1] C. W. Greeff,[1] A. L. Hungerford,[1] D. S. Montgomery,[1] D. W. Schmidt,[1]
D. G. Sheppard,[1] J. R. Williams,[1] T. R. Boehly,[2] and J. F. Benage[1,3]

[1]*Los Alamos National Laboratory, Los Alamos, New Mexico 87545, USA*
[2]*Laboratory for Laser Energetics, University of Rochester, 250 East River Road, Rochester, New York 14623, USA*
[3]*Sandia National Laboratories, Albuquerque, New Mexico 87185, USA*

We present recent results of equation-of-state (EOS) measurements of shocked silica (SiO_2) aerogel foam at the OMEGA laser facility. Silica aerogel is an important low-density pressure standard used in many high energy density experiments, including the novel technique of shock and release. Due to its many applications, it has been a heavily studied material and has a well-known Hugoniot curve. This work then complements the velocity and pressure measurements with additional temperature data providing the full EOS information within the warm dense matter regime for the temperature interval of 1–15 eV and shock velocities between 10 and 40 km/s corresponding to shock pressures of 0.3–2 Mbar. The experimental results were compared with hydrodynamic simulations and EOS models. We found that the measured temperature was systematically lower than suggested by theoretical calculations. Simulations provide a possible explanation that the emission measured by optical pyrometry comes from a radiative precursor rather than from the shock front, which could have important implications for such measurements.

PACS number(s): 52.25.Kn, 52.65.Yy, 52.65.Kj, 52.70.Kz

I. INTRODUCTION

The equation of state (EOS) of light elements at high densities and moderate temperatures falling into the warm dense matter (WDM) regime is essential to understanding the structure of Jovian planets as well as inertial confinement fusion (ICF) experiments [1–3]. In these systems, quantum degeneracy and strong interparticle forces are significant, making the theoretical description of WDM extremely challenging. Here we present results from a combination of experimental techniques used to characterize thermodynamic properties of SiO_2 aerogel foam at warm dense conditions created by a laser of variable intensity driving a strong shock.

Low density foams are utilized in a wide range of high energy density (HED) experiments and plasma-physics-related work, including laboratory astrophysics, planetary science, basic science, and shock physics, and they have also been used as pressure standards for other EOS experiments [4–11]. A particularly important use is for radiation transport experiments, where these materials have become a standard for testing our methods and approaches to understanding radiation flow [12–15]. Because many of these HED experiments are highly integrated, they must rely on simulations for the comparison to models. In many instances, the simulation results can be sensitive to uncertainties in the equation-of-state models of these low density materials, and they can be especially sensitive to material temperature and compressibility. For this reason, accurate measurements of the equation of state and especially of the temperature of the material at a given state are needed to restrict the modeling of these experiments, particularly the radiation flow experiments [12–15].

Typically, temperature information is not obtained in standard Hugoniot-type EOS experiments [16,17]. These experiments determine the internal energy, pressure, and density for materials at a given state. However, some experiments have used visible pyrometry to attempt to determine the temperature in shock experiments [18,19]. This approach was met with limited success, but at present it is generally perceived as the best alternative at moderate to low temperatures, perhaps in the range of 5 eV or less. The approach has been used in a variety of experiments and has also been successfully used at large HED laser facilities [20,21].

Based on such results, we have carried out an experimental effort to measure the temperature in shocked aerogel foam using visible pyrometry. These experiments were conducted using the OMEGA laser at the Laboratory for Laser Energetics (LLE) [22]. The experiments were carried out at previously measured Hugoniot conditions [5,6] where the energy and density of the shocked foam are well known in order to tightly constrain the equation-of-state models and the temperature measurements. We obtained temperature measurements in the range of 0.3–2 Mbar for shocked aerogel foam initially at a density of 0.2 g/cm^3. The temperature was determined by the use of streaked pyrometer (SOP) at OMEGA [20,21]. The density and pressure of the aerogel were obtained using the latest Knudson EOS [6] from shock velocity measurements by the velocity interferometer of any reflector (VISAR) at OMEGA [23]. We then compare to both a standard theoretical model and to calculations based on quantum molecular dynamics (QMD) [24] and find a disagreement between the models and our measurements. To understand the disagreement, radiation hydrodynamic simulations with high resolution using the RAGE code [25] were carried out of the shock front moving through the foam. These simulations provide an explanation for the difference between our measurements and theoretical predictions, namely that a radiative precursor precedes the shock in the foam. This results in a reduced radiative flux escaping the shock front, compromising the pyrometry measurement, and it suggests that such detailed studies may be required to understand previous experiments that use this technique, which could impact a large number of plasma physics experiments both at lasers as well as other HED facilities.

This article is divided into several sections. Section I is the introduction. The experiment is described in Sec. II. The experimental results are presented in Sec. III, which includes two subsections for VISAR and SOP analysis, respectively. Section IV then includes a comparison with equation-of state-models, hydro simulations, which included a discussion about temperature measurements, and a comparison with calculated reflectivity of the shocked aerogel within three subsections. The work is concluded in Sec. V.

II. EXPERIMENT

The experiment was carried at the 60-beam, 30-kJ OMEGA laser facility at the University of Rochester [22]. Twelve laser beams at variable intensity ranging between 5.0×10^{13} and 2.2×10^{14} W/cm^2 and a duration of 7 ns were incident onto a plastic ablator. The resultant rapid expansion of the ablated target material drives a strong shock through the remainder of the planar target sandwich of quartz and SiO$_2$ aerogel foam. This strong shock then compresses and heats the studied aerogel sample creating the desired WDM conditions. The drive beams were frequency-tripled providing the 3ω ($\lambda = 351$ nm) laser output to increase the laser-plasma coupling efficiency [26]. The beams were incident onto the target at two cones around the target normal at angles of $23°$ and $48°$, and their spatial profile was smoothed with distributed phase plates and polarization rotators [27,28].

The target and laser setup is shown in Fig. 1. The target is a "sandwich" of several materials enclosed by a 25-μm-thick gold cone which acts as a radiation shield for any direct laser light or emission from expanding plasma on the laser side that could make its way into the line of sight of the diagnostics. The target consists of a 25-μm-thick plastic (CH) ablator, 125-μm-thick α-quartz, and SiO$_2$ aerogel foam with a 40 μm step on the back side, with a total foam thickness of 100–140 μm.
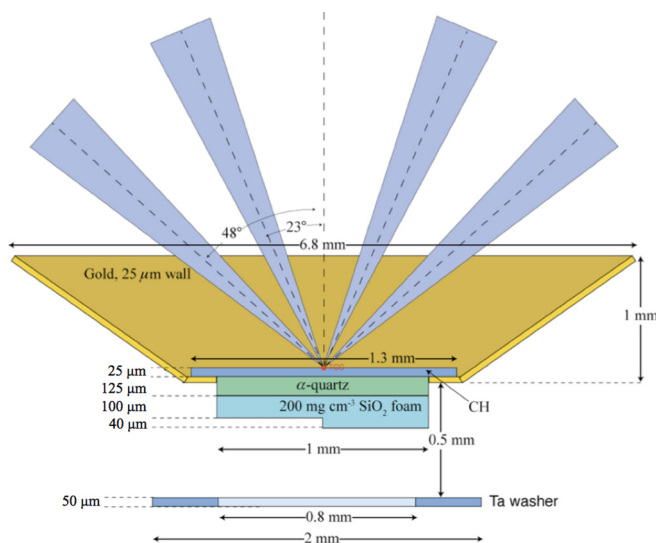

FIG. 1. (Color online) Schematic of the target setup with the laser drive coming from the top of the image incident onto a plastic ablator inside a 25-μm-thick gold cone. The target consists of a 25-μm-thick CH ablator, 125-μm-thick α-quartz, and SiO$_2$ aerogel foam with a 40 μm step on the back side (total foam thickness was 100–140 μm).

Some of the targets also had a LiF window on the back; those targets did not have any step on the foam. Each target also has a 50-μm-thick Ta washer with an 0.8-mm-wide viewing aperture to restrict the view of the velocity and temperature measurements.

The strong shock produced by the ablation of the plastic is first launched in the quartz and then transmitted into the aerogel. Quartz is a well-studied pressure standard with known EOS and thermal properties and thus excellent material to be used as a pusher in these experiments for the study of aerogel properties [21,29,30]. Another advantage of the use of α-quartz is its transparency to optical light, which is crucial for continuous shock velocity measurements by VISAR, which operates in the optical regime. The transparency of quartz was also utilized in the experiments for absolute reflectivity measurements of the silica foam [21].

The VISAR was used to directly measure the velocity of the shock wave U_s as it propagated both through the quartz and later through the foam. The line-VISAR system at the OMEGA facility consists of a laser operating at 532 nm and two interferometer arms coupled with optical streak cameras; a full description of the instrument can be found in Ref. [23]. By using two independent interferometers with different optical delays, the velocity measurements from each arm can be matched to remove the 2π phase discontinuities in fast shock measurements [23]. This system produces a continuous record of the shock velocity history as well as a one-dimensional (1D) image of the spatial profile of the shock.

The emission temperature of the shocked aerogel was measured by streaked optical pyrometry [20]. The SOP diagnostic is an absolutely calibrated optical streak camera coupled with a charge-coupled device (CCD) detector, which utilizes a series of ND filters, slits, and optical components to provide a temporally resolved record of self-emission from the shock front in a narrow wavelength band around $\lambda_0 = 684$ nm; for more details on the instrument setup, see Ref. [20]. This diagnostic records an absolutely calibrated intensity trace of the emission from the front of the shock wave with ps temporal resolution. The temperature is then extracted from the measured intensity trace within the narrow spectral window with black- or gray-body emission [20,31]. SOP has been used as a standard diagnostic to measure the temperature of plasmas for various types of experiments and materials [32–38].

III. RESULTS

A. VISAR analysis

The line-VISAR system at OMEGA was used to provide a continuous record of the shock velocity U_s evolution during the experiment both in quartz and the silica aerogel. The shock velocity was calculated from the measured phase shift recorded by each of the two interferometer arms using known parameters, and the system and analysis method is described in detail in Ref. [23]. The thermodynamics of the single shock propagating through the steady material is governed by the Hugoniot relations derived from the mass, momentum, and energy conservation across a single shock front independent of the EOS [31]. The Hugoniot relations $P = \rho_0 U_s U_p$ and $\rho = \rho_0 U_s/(U_s - U_p)$ are then used to determine the pressure
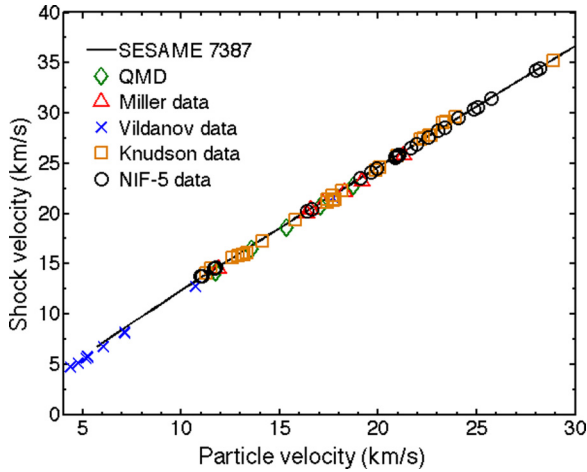
FIG. 2. (Color online) Comparison of shock and particle velocity measurements by Knudson *et al.* [5,6], Miller *et al.* [39,40], and Vildanov [41], with SESAME table 7387 [42]. Our measurements (NIF-5) of the shock velocity and calculated values of particle velocities are also included in the plot.

P and density ρ of the shocked material based on the measured initial conditions (marked with 0 subscripts) and shock velocity U_s [16,17,29].

The particle velocity U_p in shock compression experiments is usually found from the measured shock speed U_s and the EOS of a standard material by the use of impedance-matching (IM) [5,31]. The values for U_p, which are required to calculate shock pressure, can also be found using the U_p-U_s relationship for silica aerogel from SESAME table 7387 [42]: $U_s = 0.507 + 1.20274 \times U_p$, which are in excellent agreement with precise shock and particle velocities measurements by Knudson *et al.* using the IM method [5,6], which provided the relationship of $U_s = -0.45(\pm 0.17) + 1.26(\pm 0.01) \times U_p$. These relationships also agree very well with other experimental data by Miller *et al.* [39,40] and Vildanov *et al.* [41]; see Fig. 2. Our plots for each calculated value of U_p corresponding to individual shock velocity measurements from VISAR are also shown in Fig. 2. The measured range of shock velocities was 10–40 km/s, which gives us the shock pressures of 0.3–2 Mbar.

B. SOP analysis

The optical pyrometry system was used to record a temporally resolved trace of the self-emission from the front of the shock wave as it was propagating through the silica aerogel in a similar manner to the VISAR system described above [20]. At the conditions in this experiment, the shock wave is optically thick to visible light and thus the radiation temperature approaches the black-body distribution [31]. The SOP can thus be used to measure the temperature of the shocked foam by comparing the measured emission intensity with a black- or gray-body radiation distribution. In our case, the brightness temperature of the self-emission radiation approaches the temperature of the material with a finite reflectivity R value, thus the temperature of the shocked material was calculated with the gray-body approximation
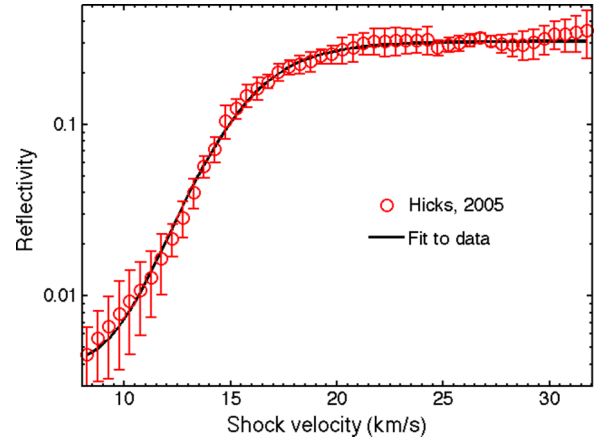

FIG. 3. (Color online) Quartz reflectivity measurement as a function of shock velocity from Ref. [21].

[31]. According to Kirchhoff's law, the absorptivity and emissivity of a gray-body are equal at any given temperature, and thus under the gray-body approximation the blackbody distribution is reduced by a constant factor $(1 - R)$, where R denotes the reflectivity [20,31]. This method of temperature measurement has been previously used for SiO_2 as well as other materials [18,19,21].

It should be noted that since the date of publication of Ref. [20], the streaked optical pyrometry instrument at OMEGA has been modified, with several optical components and the streak camera being replaced. As a result, the calibration constants have changed, however the procedure of the analysis and relations to the black- or gray-body radiation remains the same. The gray-body temperature is obtained from the expression derived in Ref. [20]:

$$T = \frac{T_0}{\ln\left[1 + (1 - R)A/I_{SOP}\right]}, \qquad (1)$$

where $T_0 = hc/\lambda_0$ is the characteristic temperature associated with the centroid of the SOP wavelength band λ_0, A is the camera signal integration constant defined in Ref. [20], R is the reflectivity of the shocked silica aerogel, and I_{SOP} is the digital
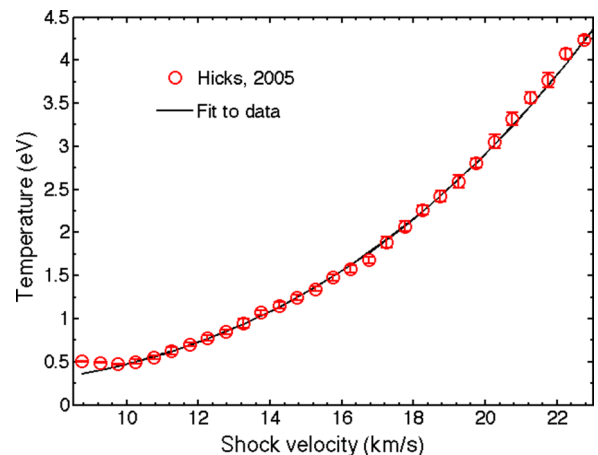

FIG. 4. (Color online) Measured temperature of shocked α-quartz as a function of shock velocity from Ref. [21].
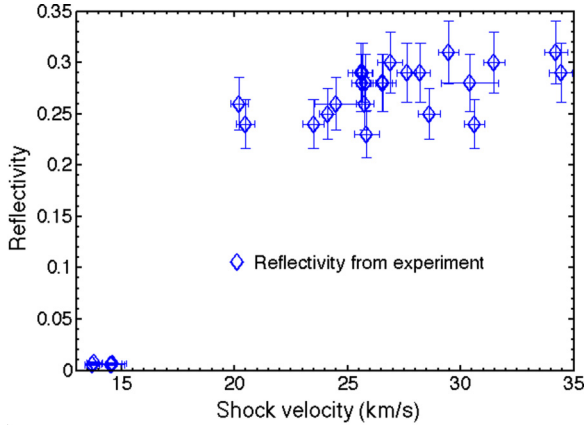
FIG. 5. (Color online) Reflectivity of silica aerogel from experiment, determined from VISAR and SOP data.

output from the SOP diagnostic as measured by the CCD. To obtain the new calibration constants T_0, A, and the reflectivity of the silica aerogel R, we used experimental data presented by Hicks *et al.* in Ref. [21], where the temperature and reflectivity of shocked α-quartz were measured as a function of shock velocity U_s. Using these data sets, we are able to obtain the reflectivity values for quartz for a given shock velocity; see Fig. 3. These values for reflectivity of shocked quartz were obtained from the Hill equation fit to the data: $R_{quartz} = R_0 + (R_m - R_0) \times U_s^n/(U_s^n + D^n)$, with constants $R_0 = 0.004$, $R_m = 0.307$, $n = 9.7$, and $D = 16.2$. Then, since the output of the VISAR laser is constant over the period of the measurement, we could use the change in intensity of the light reflected from the shock as it was breaking out from quartz to the aerogel to obtain the reflectivity in the silica aerogel foam: $R = (I_{foam}/R_{quartz}) \times I_{quartz}$.

The optical pyrometry measured both the temperature trace from the quartz as well as from the silica aerogel as the shock front was propagating through the target. The intensity trace from SOP when the shock is moving through the quartz is then used to find the constants A and T_0 as fitting parameters between Eq. (1) and the power-law fit to data measured by Hicks *et al.* in Ref. [21]: $T = T_Q + Q \times U_s^n$, where the centroid temperature $T_Q = 1400$ K, constant $Q = 4.3$, power $n = 2.98$, and U_s is the shock velocity in quartz as measured by VISAR; see Fig. 4. The average centroid temperature T_0 was found to be 5518.2 ± 35.7 K, and the instrument sensitivity constant $A = 225.2 \pm 25.9$ and 633.6 ± 36.4 for the two different experimental days, respectively. The error in temperature was estimated to be $\sim16\%$ based on the uncertainty in determination of the calibration constants, the reflectivity of the aerogel from the VISAR trace, and jitter in the data. The resultant values of R as functions of the shock velocity are shown in Fig. 5.

IV. DISCUSSION

A. Comparison to EOS models

We used the Los Alamos SESAME [42] equation of state number 7387 for SiO_2 in both hydrodynamic simulations and Hugoniot calculations. SESAME is a library of tabular

equations of state that typically cover very wide ranges of temperature and density. To accommodate this large range, the theoretical models used [42] incorporate correct limiting behavior and have enough empirical parameters to match data where they are available. Often, detail is sacrificed in favor of consistency over a wide range of states. SESAME table 7387 [43] was developed for fused quartz using primarily data from the solid and compressed liquid states corresponding to densities $\rho \geqslant 2.2$ g/cm^3.

The states of interest here for shocked aerogel lie at densities of $\rho \sim 1.1$ g/cm^3. This is between the critical density, $\rho_c = 0.508$ g/cm^3 [44], and the solid density of $\rho = 2.2$ g/cm^3. The temperatures of interest are several eV, and thus they lie above the critical temperature [44] of 0.44 eV. Electronic excitations make an important contribution to the equation of state in this range, and bond dissociation may come into play. SESAME equation of state 7387 represents the energy and pressure as a sum of cold, electronic excitation and ion motion contributions [43]. The electronic excitation term uses the Thomas-Fermi-Dirac model [45], which is smooth and lacks shell structure. The ion motion contribution is essentially an interpolation between dense fluid and dilute gas limits in this range. The EOS has no detailed representation of bond dissociation, but it does include the cohesive energy.

As a theoretical benchmark that we expect to be more predictive than the SESAME model, we have performed quantum molecular-dynamics simulations of states near the aerogel Hugoniot [46]. QMD includes the effects of bonding and electronic excitation self-consistently by simultaneously evolving the ion coordinates and the electronic states, which are described within the Kohn-Sham formulation of density functional theory [47]. Our simulations use the VASP code [46] with the PBE [48] exchange-correlation functional. We use the projector augmented wave method [49,50] with six and four electrons treated explicitly for O and Si, respectively. The plane-wave cutoff was set to 500 eV, and only the Γ point was used for Brillouin zone sums. The ion temperature was fixed using a velocity scaling thermostat, with the electron temperature [51] equal to the ion temperature. Most simulations used 72 atoms. A small number of checks with 144 atoms gave the same energy and pressure to within statistical errors. We believe the calculations to be converged with respect to numerical parameters, so that the dominant error is the approximate exchange-correlation functional. An indication of the size of this error is that simulations of α-quartz at room temperature and the experimental volume give a pressure of 3.2 GPa. The simulations were done at densities of 1.06, 1.13, and 1.20 g/cm^3, and at temperatures from 10 000 to 80 000 K in 10 000 K increments.

Hugoniot states were obtained by solving $E(V,T) - E_0 = \frac{1}{2}[P(V,T) + P_0](V_0 - V)$, where E, P, and V are the specific internal energy, pressure, and volume in the shocked state, respectively, and subscripts 0 refer to the initial state. In particular, V_0 is the porous volume. In the present calculations, E_0 was taken to be the energy of bulk amorphous silica. An amorphous configuration was generated in QMD simulations by annealing the system at liquid temperatures and quenching to room temperature several times, until the energy of the final state settled down. The pair correlation functions for this state agree well those obtained by Vashishta *et al.* [52].
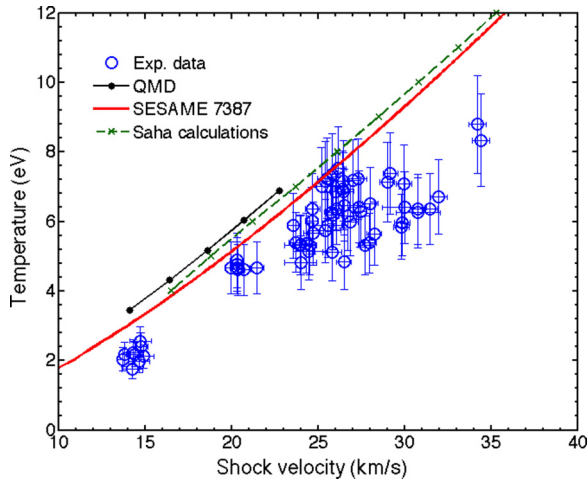
FIG. 6. (Color online) Comparison of measured temperatures as a function of shock velocity in silica aerogel with Saha calculations [53,54], our QMD simulations, and SESAME equation of state 7387 [42].

The comparison of the experimental measurements of temperatures from SOP as a function of shock velocity measured by VISAR with the quantum molecular-dynamics calculations [24], SESAME table [42], and Saha calculations [53,54] for the same shock velocities is shown in Fig. 6. There is a clear difference between the experimental data and all of the theoretical models, with the experimental temperatures being consistently lower than the theoretical predictions for the corresponding conditions. This difference gets progressively greater with increasing shock velocity. The explanation for this discrepancy is proposed in the following section.

B. Simulations and understanding the temperature observations

To understand the discrepancy between our observed temperatures and those expected in the strong shock solution, we have run a series of simulations of the experiment. For these simulations, we use the high-energy density code CASSIO developed at LANL combining the radiation adaptive grid Eulerian (RAGE) code [25] coupled with an implicit Monte Carlo treatment [55]. We model the laser source as a radiation source at the base of the experimental target. The power of this source is then varied to produce a range of drives and hence shock speeds and temperatures. With these calculations, we can calculate the particle velocity, shock velocity, shock temperature, and flux at the diagnostic for comparison with the experiment and equation-of-state data. These calculations use the SESAME equation of state in tabular form for all materials. In particular, we use the SESAME 7387 equation of state for our SiO_2 aerogel.

To get a better handle on the relevant physics in this problem, we have run a suite of models changing the physics in the code and the resolution of the silica aerogel region. We have varied the transport scheme (group structure, flux-limited diffusion versus implicit Monte Carlo) and atomic physics [decoupling of ions and electrons ("3T") and atomic levels out of thermodynamic equilibrium ("NLTE opacities")]. For the
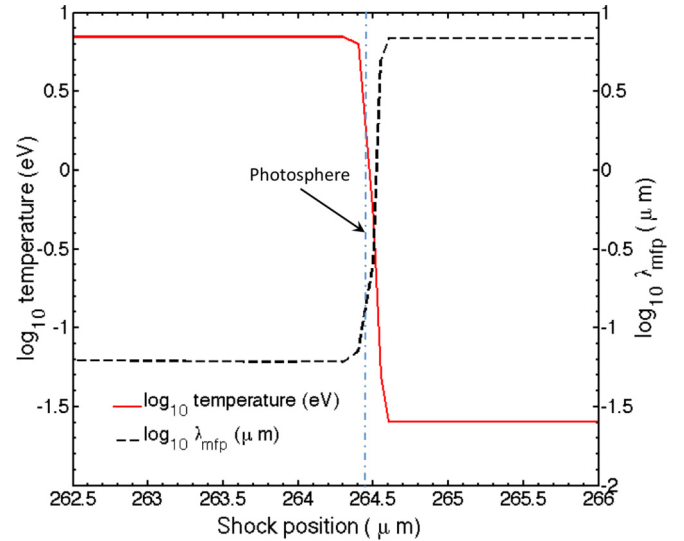

FIG. 7. (Color online) Log_{10} temperature (solid line) and log_{10} mean free path (λ_{mfp}) as a function of position for the shock 1.1 ns after the start of the laser drive. The transition region is quite narrow, but it persists even when our simulation resolution drops below 0.15 μm. The fact that this is only a few zones thick implies that numerical diffusion (despite the steepener in the RAGE code) could be the dominant effect. However, we do expect some radiative preheat, and a portion of this preheat is likely due to this radiative heating. The position of the photosphere is marked by a vertical dot-dashed line.

most part, these variations had no effect on the results. The flux-limited diffusion simulation lost more energy, driving a weaker shock, but this lower energy mimicked a lower-energy drive for the implicit Monte Carlo simulation. We have also run a broad suite of simulations with resolutions from 2.5 μm down to 0.15 μm. These simulations converged on the shock velocity, shock temperature, and flux at the diagnostic at 0.3 μm.

Figure 7 shows the temperature profile at the shock front 11 ns after the start of the energy deposition. Leading the shock is a narrow preheated region. This preheated region plays a significant role in determining the flux at the diagnostic. The Rosseland mean free path for photons is also shown in Fig. 7. It is in this preheated region that the material becomes optically thick, and the "photosphere" of the shock is in this region. Our diagnostic measures the flux, and the flux-inferred temperature, at this photosphere. This flux-inferred temperature is much lower than the shock temperature. Understanding our diagnostic results requires understanding the nature of this preheated region.

The preheating ahead of the shock can occur for a variety of reasons: nonthermal and thermal particles and photons can diffuse ahead (or "break out") of the shock, heating the material above the shock. Numerical diffusion can also artificially preheat the material just ahead of the shock. To distinguish these physical and numerical effects, we have run a series of convergence studies and analytic tests.

Although nonthermal particles are produced by the laser, the high optical depth in our ablator and α-quartz will thermalize these photons before they reach the shock front

in the foam. Photons and ions at the shock front can diffuse ahead of the shock. In astrophysics, this diffusion is termed "shock breakout," and we will use the astrophysics formalism to test the importance of this diffusion. Breakout occurs when the shock velocity is less than the diffusion velocity $v_{\mathrm{diffusion}}$ at the front:

$$v_{\mathrm{diffusion}} = \Delta x/t_{\mathrm{diffusion}} = v_{\mathrm{ion}}/(\Delta x \sigma \rho), \qquad (2)$$

where Δx is the width of the preheated region (to compare to our numerical resolution, we set Δx to the cell size at the shock front $\sim 10^{-5}$ cm) and $t_{\mathrm{diffusion}} = (\Delta x/\lambda)^2 \lambda/v_{\mathrm{ion}}$ is the diffusion time. $\lambda = (\sigma \rho)^{-1}$ is the mean free path, where ρ is the number density of ions at our shock front ($\sim 3 \times 10^{21}$ cm^{-3}) and, for typical electron/ion collisions in the 3–15 eV range, the cross section $\sigma \approx (1–10) \times 10^{-16}$ cm^2 [56]. For our strong shocks, the ion velocity, v_{ion}, is on a par with the shock velocity. Using these quantities, we find $v_{\mathrm{diffusion}} < 0.1 v_{\mathrm{shock}}$. Any diffusion is slower than the shock velocity, and the ions are trapped in the shock.

Radiative diffusion is a different matter. Using the speed of light for the particle velocity, and incorporating the high shock opacities (2×10^5 cm^2 g^{-1}), we find the diffusion velocity to be greater than the shock velocity, and we expect, as we see in our simulations, a radiative precursor to the shock. This radiation interacts with the matter ahead of the shock, producing the precursor in front of this shock. This material interaction raises the opacity, and the effective "photosphere" of the shock lies within this precursor, causing the observed temperature to be lower than that of the shock itself.

Although we expect some preheating, the question remains for our simulations just how much of the preheat is caused by radiation versus numerical diffusion. Our resolution study was designed to answer this question. As we increased our resolution, we sought convergence on a number of quantities: shock speed, shock temperature, and flux-inferred temperature at the diagnostic. At 0.3 μm, the simulation converged and we saw no further changes ($<1\%$) at 0.15 μm. For our comparisons with data, we use a suite of simulations with 0.3 μm resolution. At 0.15 μm, our resolution is on a par with the mean free path, but the shock front is less than 10 zones thick, and we cannot rule out that numerical diffusion in our hydrodynamics package is affecting our results.

An additional influence on the radiative precursor may be an increased mean free path of the photons due to the finite cell size of the aerogel foam. Radiation transport through porous or stochastic media has been studied for a broad range of applications [57,58]. Although how this medium affects the radiation transport depends upon the exact details of the porosity, the generic trend is that porosity increases the radiative fluence through the material over a homogeneous medium [57]. Although physics effects not included in these studies may still alter this trend, the current theoretical studies suggest that the effective mean free path of photons is increased due to the porosity of the silica aerogel.

C. Reflectivity of shocked silica aerogel

The electrical frequency-dependent conductivity was calculated via the Kubo-Greenwood formalism using Kohn-Sham orbitals, eigenvalues, and velocity dipole matrix elements from
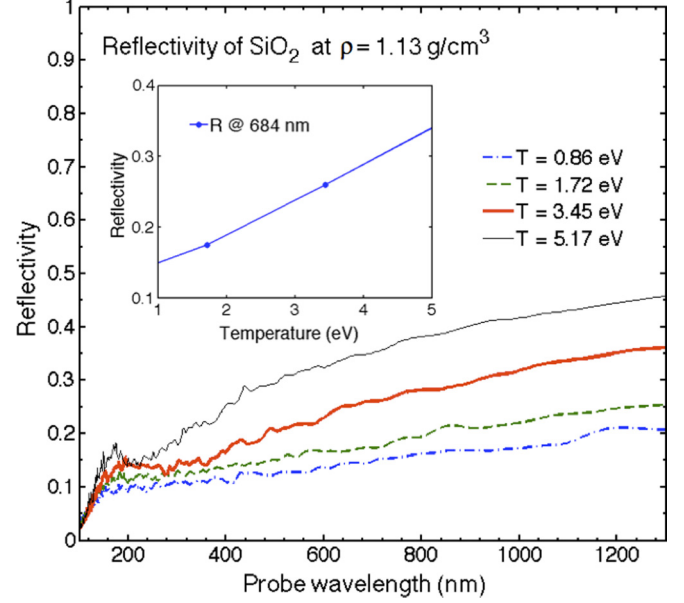

FIG. 8. (Color online) Reflectivity of silica aerogel for various conditions along the principal Hugoniot calculated using QMD simulations [24]. The optical pyrometry measurement is carried out at a narrow wavelength band around $\lambda_0 = 684$ nm.

DFT calculations [59,60]. From the real and imaginary parts of electrical conductance, the frequency-dependent dielectric functions, indices of refraction, and reflectivity are determined [61]. Optical calculations were performed using configurational snapshots from QMD runs with a $2 \times 2 \times 2$ Monkhorst-Pack mesh [62], and reflectivity reported is averaged over two to five snapshots.

Figure 8 shows reflectivity at a density of $\rho = 1.13$ g/cm^3 and temperatures of $T = 0.86$ eV (10 000 K), 1.72 eV (20 000 K), 3.45 eV (40 000 K), and 5.17 eV (60 000 K). At the experimental wavelength ($\lambda_0 = 684$ nm), reflectivity is linear over the calculated temperature range shown in the inset of Fig. 8. Calculated reflectivity changes with respect to density around the Hugoniot were insignificant. Excellent experimental agreement with calculations was found for moderate velocities. For lower temperatures, calculated reflectivity was higher than experimental.

The reflectivity measurements from the experiment are consistent with these theoretical calculations for temperatures above 3 eV and shock velocities above 20 km/s. A strong inconsistency is observed for lower shock velocities (temperatures below 2 eV), where the theory predicts reflectivities between 0.1 and 0.2 (see the inset in Fig. 8), while the numbers obtained from experiment were significantly lower, by two orders of magnitude, as shown in Fig. 5. This also influences the data analysis for the temperature determination. Using the calculated R rather than the experimentally determined values for these low shock velocities would shift the lower end data closer to the theoretical predictions by $\sim 15\%$. This is not a significant difference, and it has little effect on the final result, but it deserves further investigation. At this point, this discrepancy between the theoretical calculations and experimental measurements of R for the lower temperatures

and shock velocities is attributed to the very low reflected light signals from those measurements. These low signals call into question the accuracy and normalization of the reflectivity for the low velocities.

V. CONCLUSIONS

We have completed a set of temperature measurements for shocked aerogel foams at states along the principal Hugoniot for an initial density of 0.2 g/cm^3. These measurements used a standard streaked optical pyrometry approach, and the results indicate that the measured temperature falls below the value expected for a standard SESAME equation-of-state table that predicts the Hugoniot behavior well. More importantly, the results fall below temperatures expected from QMD calculations that we believe are accurate [63] for such conditions, and the discrepancy increases as the pressure increases. Since SOP has become a standard technique to measure temperature in moving shock fronts in a wide variety of plasma physics, ICF, equation-of-state, material, and planetary science experiments, an investigation of such a phenomenon is of a great importance to many experimentalists as well as theorists [21,32–38].

To resolve this, we completed a series of highly resolved simulations that explored the details of the shock propagation in the foam coupled with the emission from the shock front. These simulations indicate that a radiative precursor propagates ahead of the shock into the unshocked foam, which then emits radiation at the photon energies measured by the diagnostic. This thin, radiative precursor layer exists at a reduced temperature from the bulk of the shocked material and thus reduces the corresponding temperature interpreted from the radiation.

The dominant physical mechanism producing this effect is the relatively long mean free path of the radiation from the shock compared to the measured radiation. What is somewhat surprising is that this discrepancy occurs at even the lowest temperatures measured, around 2–3 eV. At lower shock velocities, the result is affected by the lower value of aerogel reflectivity. If the value of R is corrected using the quantum molecular-dynamics calculations, the resultant temperatures from SOP will lie closer to the QMD and SESAME equation of state at temperatures below 3 eV.

Although we are confident that the simulations have captured the general behavior of the radiation, some detailed issues remain. In the simulations, it was found that in addition to radiation, numerical diffusion contributed to the preheated region. Evenhough this is a numerical artifact, it may be mimicking the realistic longer mean free paths that occur due to the porosity of the unshocked foam. How important these issues are for nonporous materials and other optical pyrometry measurements is a matter for future investigation.

[1] T. Guillot, Science **286**, 72 (1999).

[2] J. Nuckolls *et al.*, Nature (London) **239**, 139 (1972).

[3] R. L. McCrory *et al.*, Nucl. Fusion **45**, S283 (2005).

[4] M. D. Knudson *et al.*, Phys. Rev. Lett. **87**, 225501 (2001).

[5] M. D. Knudson, J. R. Asay, and C. Deeney, J. Appl. Phys. **97**, 073514 (2005).

[6] M. D. Knudson and R. W. Lemke, J. Appl. Phys. **114**, 053510 (2013).

[7] K. Falk, E. J. Gamboa, G. Kagan, D. S. Montgomery, B. Srinivasan, P. Tzeferacos, and J. F. Benage, Phys. Rev. Lett. **112**, 155003 (2014).

[8] K. Falk *et al.*, Phys. Plasmas **21**, 056309 (2014).

[9] M. K. Matzen, Phys. Plasmas **4**, 1519 (1997).

[10] N. Holmes, *High-Pressure Science and Technology—1993* (AIP, New York, 1994), p. 153.

[11] X. Zhu *et al.*, Fusion Eng. Design **87**, 92 (2012).

[12] E. Falize, C. Michaut, and S. Bouquet, Astrophys. J. **730**, 96 (2011).

[13] P. A. Rosen *et al.*, Astrophys. Space Sci. **322**, 101 (2009).

[14] T. E. Tierney IV *et al.*, Rev. Sci. Instrum. **79**, 10E919 (2008).

[15] A. Moore *et al.*, *54th Annual Meeting of the APS DPP*, abstract no. CO4.010 (APS, New York, 2012).

[16] M. D. Knudson *et al.*, J. Phys. A **36**, 6149 (2003).

[17] M. D. Knudson, D. L. Hanson, J. E. Bailey, C. A. Hall, J. R. Asay, and C. Deeney, Phys. Rev. B **69**, 144209 (2004).

[18] G. W. Collins *et al.*, Phys. Rev. Lett. **87**, 165504 (2001).

[19] J. E. Bailey, M. D. Knudson, A. L. Carlson, G. S. Dunham, M. P. Desjarlais, D. L. Hanson, and J. R. Asay, Phys. Rev. B **78**, 144107 (2008).

[20] J. E. Miller *et al.*, Rev. Sci. Instrum. **78**, 034903 (2007).

[21] D. G. Hicks, T. R. Boehly, J. H. Eggert, J. E. Miller, P. M. Celliers, and G. W. Collins, Phys. Rev. Lett. **97**, 025502 (2006).

[22] T. R. Boehly *et al.*, Opt. Commun. **133**, 495 (1997).

[23] P. M. Celliers *et al.*, Rev. Sci. Instrum. **75**, 4916 (2004).

[24] G. Kresse and J. Hafner, Phys. Rev. B **47**, 558(R) (1993).

[25] M. Gittings *et al.*, Comput. Sci. Disc. **1**, 015005 (2008).

[26] W. L. Kruer, *The Physics of Laser Plasma Interactions* (Westview, Colorado, 2003).

[27] Y. Lin, T. J. Kessler, and G. N. Lawrence, Opt. Lett. **20**, 764 (1995).

[28] S. P. Regan *et al.*, J. Opt. Soc. Am. B **22**, 998 (2005).

[29] D. G. Hicks *et al.*, Phys. Plasmas **12**, 082702 (2005).

[30] T. R. Boehly, J. E. Miller, D. D. Meyerhofer, J. H. Eggert, P. M. Celliers, D. G. Hicks, and G. W. Collins, in *Proceedings of the Conference of the American Physical Society Topical Group on Shock Compression of Condensed Matter*, edited by M. Elert, M. D. Furnish, R. Chau, N. Holmes, and J. Nguyen, AIP Conf. Proc. No. 955 (AIP, New York, 2007), p. 19.

[31] Y. B. Zel'dovich and Y. P. Raizer, *Physics of Shock Waves and High Temperature Hydrodynamic Phenomena* (Dover, Mineola, NY, 2002).

[32] J. H. Eggert *et al.*, Nat. Phys. **6**, 40 (2010).

[33] T. R. Boehly, V. N. Goncharov, W. Seka, M. A. Barrios, P. M. Celliers, D. G. Hicks, G. W. Collins, S. X. Hu, J. A. Marozas, and D. D. Meyerhofer, Phys. Rev. Lett. **106**, 195005 (2011).

[34] G. Huser *et al.*, Phys. Plasmas **12**, 060701 (2005).

[35] G. M. Dyer *et al.*, Phys. Rev. Lett. **101**, 015002 (2008).

[36] N. Ozaki *et al.*, Phys. Plasmas **16**, 062702 (2009).

[37] R. E. Olson *et al.*, Phys. Rev. Lett. **91**, 235002 (2003).

[38] C. S. Yoo *et al.*, Phys. Rev. Lett. **70**, 3931 (1993).

[39] J. E. Miller, Ph.D. thesis, University of Rochester, 2007.

[40] J. E. Miller, T. R. Boehly, D. D. Meyerhofer, and J. H. Eggert, in *Proceedings of the Conference of the American Physical Society Topical Group on Shock Compression of Condensed Matter*, edited by M. Elert, M. D. Furnish, R. Chau, N. Holmes, and J. Nguyen, AIP Conf. Proc. No. 955 (AIP, New York, 2007), p. 71.

[41] V. G. Vildanov, M. M. Gorshkov, and K. K. Krupnikov, RFNC-VNIITF Report VINITI G83219, 1987.

[42] S. P. Lyon and J. D. Johnson, Los Alamos National Laboratory Report LA-UR-92-3407 (1992), http://library.lanl.gov/cgi-bin/getfile?00612717.pdf.

[43] J. C. Boettger, Los Alamos National Laboratory Report LA-12841-MS (1994), http://library.lanl.gov/cgi-bin/getfile?00296704.pdf.

[44] R. G. Kraus, S. T. Stewart, D. C. Swift, C. A. Bolme, R. F. Smith, S. Hamel, B. D. Hammel, D. K. Spaulding, D. G. Hicks, J. H. Eggert, and G. W. Collins, J. Geophys. Res.-Planets **117**, E09009 (2012).

[45] J. F. Barnes, Phys. Rev. **153**, 1 (1967).

[46] G. Kresse and J. Furthmüller, Phys. Rev. B **54**, 11169 (1996).

[47] W. Kohn and L. J. Sham, Phys. Rev. **140**, A1133 (1965).

[48] J. P. Perdew, K. Burke, and M. Ernzerhof, Phys. Rev. Lett. **77**, 3865 (1996).

[49] P. E. Blöchl, Phys. Rev. B **50**, 17953 (1994).

[50] G. Kresse and D. Joubert, Phys. Rev. B **59**, 1758 (1999).

[51] R. M. Wentzcovitch, J. L. Martins, and P. B. Allen, Phys. Rev. B **45**, 11372 (1992).

[52] P. Vashishta, R. K. Kalia, J. P. Rino, and I. Ebbsjö, Phys. Rev. B **41**, 12197 (1990).

[53] C. A. Rouse, Astrophys. J. **139**, 339 (1964).

[54] H. R. Griem, *Plasma Spectroscopy* (McGraw-Hill, New York, 1964).

[55] T. J. Urbatsch and T. M. Evans, Los Alamos National Laboratory Report LA-14195-MS (2005).

[56] A. Zecca, G. P. Karwasz, and R. S. Brusa, Riv. Nuovo Cimento **19**, 1 (1996).

[57] E. D. Fichtl and A. K. Prinja, J. Quant. Spectrosc. Radiat. Transf. **112**, 646 (2011).

[58] J. S. Cassell and M. M. R. Williams, Ann. Nucl. Energy **35**, 790 (2008).

[59] M. P. Desjarlais, J. D. Kress, and L. A. Collins, Phys. Rev. E **66**, 025401 (2002).

[60] L. A. Collins, S. R. Bickham, J. D. Kress, S. Mazevet, T. J. Lenosky, N. J. Troullier, and W. Windl, Phys. Rev. B **63**, 184110 (2001).

[61] S. Mazevet *et al.*, High Energy Density Phys. **6**, 84 (2010).

[62] H. J. Monkhorst and J. D. Pack, Phys. Rev. B **13**, 5188 (1976).

[63] M. D. Knudson and M. P. Desjarlais, Phys. Rev. Lett. **103**, 225501 (2009).